NAVAL AIR WARFARE CENTER AIRCRAFT DIVISION
PATUXENT RIVER, MARYLAND

TECHNICAL REPORT

REPORT NO: NAWCADPAX/TR-2008/3

FOREIGN OBJECT DAMAGE BY STEEL BALL PROJECTILES IN A SiC/SiC CERAMIC MATRIX COMPOSITE AT AMBIENT AND ELEVATED TEMPERATURES

by

Sung R. Choi
Donald J. Alexander

29 April 2008

Approved for public release; distribution is unlimited.

DEPARTMENT OF THE NAVY
NAVAL AIR WARFARE CENTER AIRCRAFT DIVISION
PATUXENT RIVER, MARYLAND

NAWCADPAX/TR-2008/3
29 April 2008

FOREIGN OBJECT DAMAGE BY STEEL BALL PROJECTILES IN A SiC/SiC CERAMIC MATRIX COMPOSITE AT AMBIENT AND ELEVATED TEMPERATURES

by

Sung R. Choi
Donald J. Alexander

RELEASED BY:

_____ 29 Apr 2008
STEPHEN J. SPADAFORA / AIR-4.3.4 / DATE
Head, Materials Engineering Division
Naval Air Warfare Center Aircraft Division

REPORT DOCUMENTATION PAGE			Form Approved OMB No. 0704-0188		
Public reporting burden for this collection of information is estimated to average 1 hour per response, including the time for reviewing instructions, searching existing data sources, gathering and maintaining the data needed, and completing and reviewing this collection of information. Send comments regarding this burden estimate or any other aspect of this collection of information, including suggestions for reducing this burden, to Department of Defense, Washington Headquarters Services, Directorate for Information Operations and Reports (0704-0188), 1215 Jefferson Davis Highway, Suite 1204, Arlington, VA 22202-4302. Respondents should be aware that notwithstanding any other provision of law, no person shall be subject to any penalty for failing to comply with a collection of information if it does not display a currently valid OMB control number. **PLEASE DO NOT RETURN YOUR FORM TO THE ABOVE ADDRESS.**					
1. REPORT DATE 29 April 2008		2. REPORT TYPE Technical Report	3. DATES COVERED FY07-FY08		
4. TITLE AND SUBTITLE Foreign Object Damage by Steel Ball Projectiles in a SiC/SiC Ceramic Matrix Composite at Ambient and Elevated Temperatures			5a. CONTRACT NUMBER		
			5b. GRANT NUMBER		
			5c. PROGRAM ELEMENT NUMBER		
6. AUTHOR(S) Sung R. Choi Donald J. Alexander			5d. PROJECT NUMBER		
			5e. TASK NUMBER		
			5f. WORK UNIT NUMBER		
7. PERFORMING ORGANIZATION NAME(S) AND ADDRESS(ES) Naval Air Warfare Center Aircraft Division 22347 Cedar Point Road, Unit #6 Patuxent River, Maryland 20670-1161			8. PERFORMING ORGANIZATION REPORT NUMBER NAWCADPAX/TR-2008/3		
9. SPONSORING/MONITORING AGENCY NAME(S) AND ADDRESS(ES) Naval Air Systems Command 47123 Buse Road Unit IPT Patuxent River, Maryland 20670-1547			10. SPONSOR/MONITOR'S ACRONYM(S)		
			11. SPONSOR/MONITOR'S REPORT NUMBER(S)		
12. DISTRIBUTION/AVAILABILITY STATEMENT Approved for public release; distribution is unlimited.					
13. SUPPLEMENTARY NOTES					
14. ABSTRACT Foreign object damage (FOD) phenomenon of a gas-turbine grade SiC/SiC ceramic matrix composite was determined at 25°C and 1316°C using impact velocities ranging from 115 to 440 m/sec by 1.59-mm diameter steel ball projectiles. Two types of target-specimen support were employed at each temperature: fully supported and partially supported. For a given temperature, the degree of post-impact strength degradation increased with increasing impact velocity, and was greater in a partially supported configuration than in a fully supported one. The elevated-temperature FOD resistance of the composite, particularly in partial support at higher impact velocities ≥350 m/sec, was significantly less than the ambient-temperature counterpart, attributed to a weakening effect of the composite. In full support, frontal contact stress played a major role in generating composite damage; whereas, in partial support, both frontal contact and backside flexure stresses were combined sources of damage generation. Formation of cone cracks initiating from impact site was also one of the key damage aspects. The SiC/SiC composite was able to survive higher energy impacts without complete structural failure, as compared to gas-turbine grade AS800 and SN282 monolithic silicon nitrides.					
15. SUBJECT TERMS melt-infiltrated (MI); SiC/SiC ceramic matrix composite (CMC); foreign object damage (FOD); mechanical testing; impact					
16. SECURITY CLASSIFICATION OF:			17. LIMITATION OF ABSTRACT	18. NUMBER OF PAGES	19a. NAME OF RESPONSIBLE PERSON Sung R. Choi
a. REPORT	b. ABSTRACT	c. THIS PAGE			19b. TELEPHONE NUMBER (include area code)
Unclassified	Unclassified	Unclassified	SAR	40	301-342-8074; sung.choi1@navy.mil

Standard Form 298 (Rev. 8-98)
Prescribed by ANSI Std. Z39-18

SUMMARY

Foreign object damage (FOD) phenomenon of a gas-turbine grade SiC/SiC ceramic matrix composite was determined at 25°C and 1316°C using impact velocities ranging from 115 to 440 m/sec by 1.59-mm diameter steel ball projectiles. Two types of target-specimen support were employed at each temperature: fully supported and partially supported. For a given temperature, the degree of post-impact strength degradation increased with increasing impact velocity, and was greater in a partially supported configuration than in a fully supported one. The elevated-temperature FOD resistance of the composite, particularly in partial support at higher impact velocities $\geq$350 m/sec, was significantly less than the ambient-temperature counterpart, attributed to a weakening effect of the composite. In full support, frontal contact stress played a major role in generating composite damage; whereas, in partial support, both frontal contact and backside flexure stresses were combined sources of damage generation. Formation of cone cracks initiating from impact site was also one of the key damage aspects. The SiC/SiC composite was able to survive higher energy impacts without complete structural failure, as compared to gas-turbine grade AS800 and SN282 monolithic silicon nitrides.

Contents

ACKNOWLEDGEMENTS

1. INTRODUCTION

Ceramics, because of their brittle nature, are susceptible to localized surface damage/cracking when subjected to impact by foreign objects. It is also true that ceramic components may fail structurally even by soft particles when the kinetic energy of impacting objects exceeds certain limits. Therefore, foreign object damage (FOD) associated with particle impact needs to be considered when ceramic materials are designed for structural applications such as gas-turbine airfoils. In view of this importance, a considerable amount of work on impact damage of brittle materials by sharp particles as well as by blunt particles or by plates has been performed both experimentally and analytically, including the assessments of FOD for turbine engine applications (references 1 through 14). Examples of metallic turbine airfoils with thermal barrier coatings (TBCs) that encountered FOD are shown in figure 1. Spallation of TBCs from the substrates by some impacting particles is evident. Prospective impact damage will be certainly amplified if the turbine components were made of ceramics or ceramic matrix composites due to their brittleness.
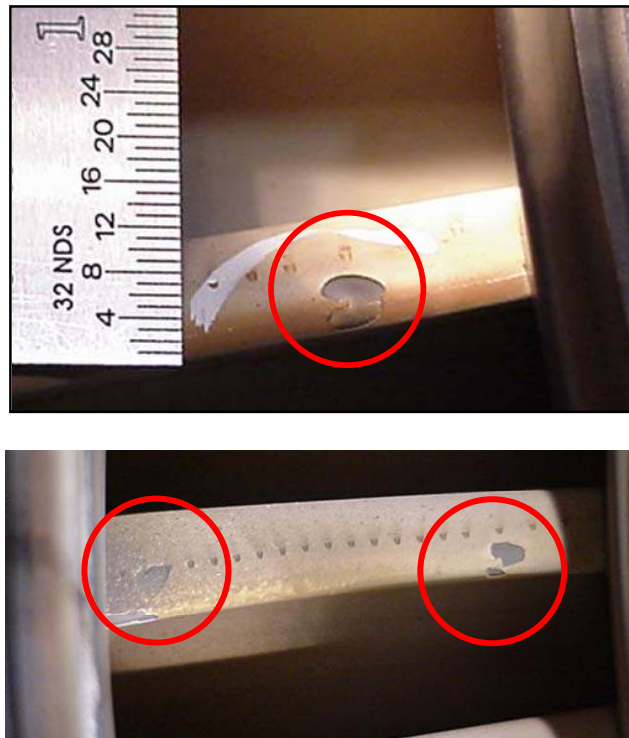

Figure 1: Examples of airfoils subjected to FOD by impacting particles.
(Courtesy: Joel Pratter, Jacksonville)

In previous studies (references 15 and 16), FOD behavior of two representative gas-turbine grade silicon nitrides, AS800 and SN282, was determined at ambient temperature using both flexure bars and disks. Fully supported ceramic target specimens were impacted at their centers

by steel ball projectiles with a diameter of 1.59 mm in a velocity range from 220 to 440 m/sec. AS800 silicon nitride exhibited a greater FOD resistance than SN282, due to its greater value of fracture toughness (K_{Ic}). Multiple crack systems were generated in the target specimens at higher impact velocities. A fracture map was proposed to identify particular crack systems as a function of impact velocity. The FOD work was also extended to cover the effect of projectile materials on FOD in a silicon nitride using hardened and annealed steel, brass, and ceramic balls (reference 17).

The present work, as a continuation of the previous studies, explores FOD phenomenon of a gas-turbine grade, silicon carbide fiber-reinforced silicon carbide ceramic matrix composite (SiC/SiC). This 2-D woven SiC/SiC ceramic matrix composite (CMC) has shown good elevated-temperature strength, creep and rupture properties, and good thermal conductivity. However, like any other materials, there are a few properties and behaviors that are required to be evaluated before the material is put into applications. One of those properties and behaviors is how FOD influences the mechanical degradation of the composite at temperatures close to typical operating or target temperatures of structural components. For this purpose, SiC/SiC CMC target specimens with a flexure bar configuration were impacted at velocities ranging from 115 to 440 m/sec by 1.59-mm diameter steel ball projectiles at both 25°C and 1316°C. Two different types of specimen support, fully supported and partially supported, were employed at each temperature. Post-impact strength of each target specimen impacted was determined as a function of impact velocity to assess the severity of impact damage. Fractography was performed before and after post-impact strength testing to determine impact-damage morphologies. A quasi-static model to predict the impact force and backside tensile stress in partial support was also proposed and assessed with experimental observations. Some preliminary results on this work have been reported previously (reference 18).

2. EXPERIMENTAL PROCEDURES

2.1 MATERIAL AND TEST SPECIMENS

The material used in this work was 2-D woven Sylramic™, BN interface, melt-infiltrated (MI) SiC CMC. The composite was fabricated by GE Power System Composites (Newark, DL; vintage '02). Briefly, Sylramic™ SiC fibers, produced in tow form by Dow Corning (Midland, Michigan) were woven into 2-D 5 harness-satin cloth and then converted to Sylramic iBN fibers. The Sylramic iBN cloth was cut into 230 x 150 mm plies, which were 8 ply-stacked and chemically vapor infiltrated with a thin BN-based interface coating followed by SiC matrix over-coating. Remaining matrix porosity was filled with SiC particulates and then with molten silicon. The composite was composed of about 34 vol% SiC fibers, about 5 vol% BN coating, and about 61 vol% SiC coating, SiC particulates, silicon and pores. The nominal dimensions of each panel thus fabricated were about 230 mm by 150 mm with a thickness of about 2.2 mm. Typical microstructure of the composite is shown in figure 2. The panels were machined into flexure beams for FOD testing, measuring 8 mm in width, 45 mm in length, and 2.2 mm in as-furnished thickness.
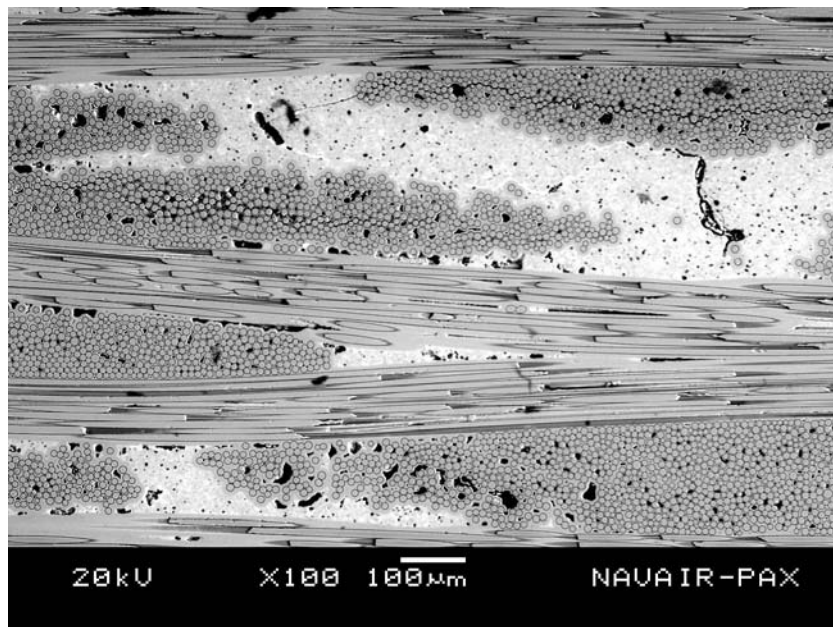

Figure 2: Microstructure of SiC/SiC CMC used in this work.

2.2 FOREIGN OBJECT DAMAGE TESTING

FOD testing was conducted at both ambient and elevated temperatures using the experimental apparatus shown in figure 3. Detailed descriptions of the apparatus can be found elsewhere (references 15 and 16). Hardened (HRC≥60) chrome steel balls with a diameter of 1.59 mm were inserted into a 300-mm long gun barrel with an inner diameter of 1.59 mm. A

2000 psi helium gas cylinder and relief valves were used to pressurize the reservoir to a specific level, depending on prescribed impact velocity. Upon reaching a specific level of pressure, a solenoid valve was instantaneously opened accelerating a steel ball projectile through the gun barrel to impact a target specimen. The target specimen was fully or partially supported through a SiC specimen holder, as shown in figure 4. The reason for use of these two different supports stems from a prospective CMC airfoil's configurations and a random nature of impact by projectiles, as illustrated in figure 5. Various types of support system can be considered, depending on the configuration of airfoils and their attachment to neighboring components. However, any configuration would fall into a category between the full and partial supports. A partially supported system certainly gives rise to a conservative approach.
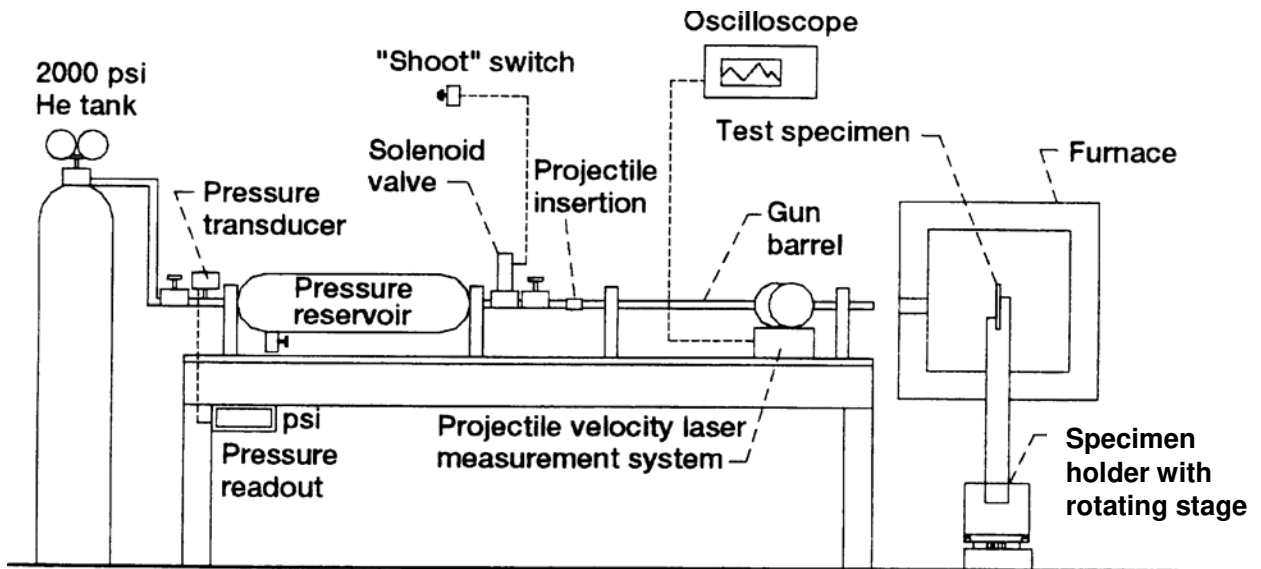
Figure 3: FOD testing apparatus with a high-temperature furnace (references 15 and 16).
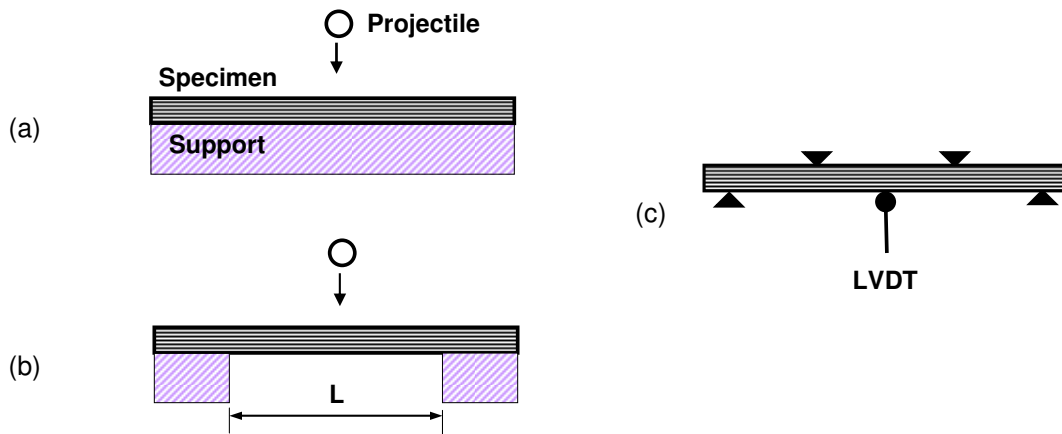
Figure 4: Two types of target specimen support used in FOD testing: (a) fully supported and (b) partially supported (L=20 mm) configurations; (c) four-point flexure test configuration used in post-impact strength testing for impacted specimens with a linear variable displacement transformer (LVDT) placed at midpoint.

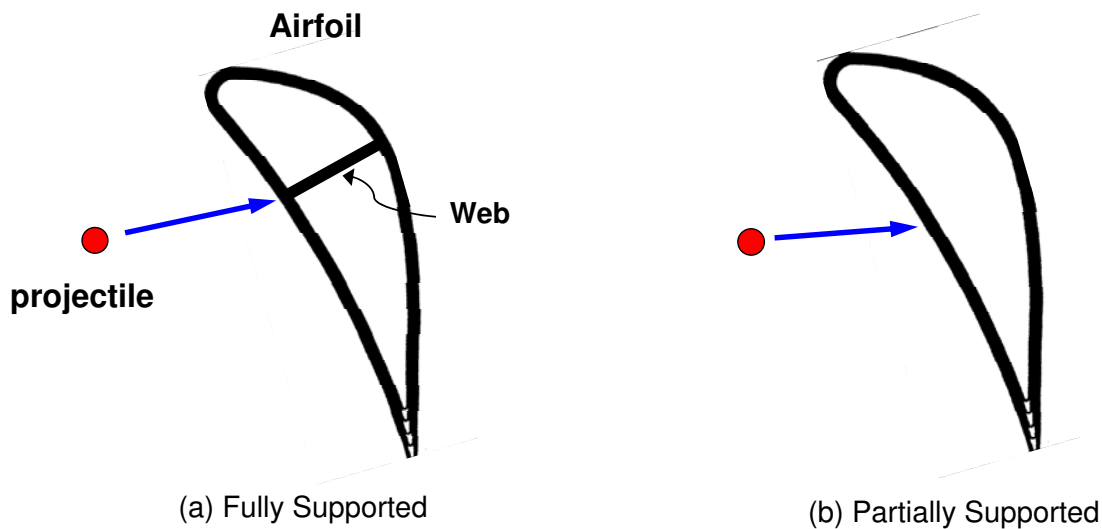

(a) Fully Supported

(b) Partially Supported

Figure 5: Airfoils with respect to impacting projectiles giving rise to: (a) fully supported and (b) partially supported conditions.

Each target specimen in figure 4 was aligned such that the projectile impacted at the center of the specimen with a normal incidence angle. Two different temperatures of 25°C and 1316°C (or 2400°F) were used for each type of specimen support. In elevated-temperature testing, a target specimen was assembled together with the SiC holder outside of a furnace, and then the target specimen-SiC holder assembly was slowly (to minimize thermal shock) raised up via a DC

servo motor feed mechanism into the furnace whose temperature was slightly below the test temperature. The specimen was then heated, held at the test temperature for about 15 min for thermal equilibration, and subjected to projectile impact. A thermocouple was placed close to the target specimen to monitor and control temperature. After impact testing, the specimen was slowly lowered from the furnace and taken out of the holder assembly for subsequent examination and testing.

Impact velocity of each projectile was determined using two pairs of laser transmitter and receiver, incorporated with two holes in the gun barrel, as previously described (reference 16). The range of impact velocity employed in this work was from 115 to 440 m/sec. One to three test specimens were used at each velocity for a given specimen support. Impact damage morphologies of target specimens were examined by optical and scanning electron microscopy prior to post-impact strength testing. Cross-sections of some of the selected specimens impacted at high velocities (around 400 m/sec) in partial support were also examined to better understand their associated impact/failure mechanisms.

2.3 POST-IMPACT STRENGTH TESTING

Strength testing for target specimens impacted from 115 to 400 m/sec was carried out at ambient temperature in air to determine the severity of impact damage using a four-point flexure fixture with 20-mm inner and 40-mm outer spans (see figure 3). Each impacted specimen was loaded in the flexure fixture such that its impact site was subjected to tension within the inner span. An LVDT was used to determine the center deflection of specimens during testing. An electromechanical test frame (Model 8562, Instron, Canton, Massachusetts) was used in displacement control with an actuator speed of 0.5 mm/min. As-received flexural strength was also determined for a baseline data using three test specimens, incorporated with the same test fixture, test frame, and test conditions that were employed in the post-impact strength testing.

3. RESULTS AND DISCUSSION

3.1 IMPACT DAMAGE MORPHOLOGY

Most of steel ball projectiles were plastically deformed (flattened) upon impact with their degree of deformation being dependent on impact velocity. At higher impact velocities (>350 m/sec), some of the projectiles were subjected to extreme heat evidenced by discoloration or fractured into pieces. However, it was observed that the overall projectile damage was less in the composite than in AS800 and SN282 monolithic silicon nitrides (references 15 and 16), since elastic modulus (E) was much lower in the composite (E=220 GPa) than in the silicon nitrides (E=340 GPa) and since the degree of projectile deformation for a given specimen support depends on elastic modulus of a target material. Note that elastic modulus of brittle materials is also a measure of hardness; the stiffer, the harder, and vice versa. Projectiles impacted SiC/SiC and AS800 silicon nitride target specimens at 350 m/sec are shown in figure 6, where the extent of plastic deformation is easily distinguishable between the two projectiles.

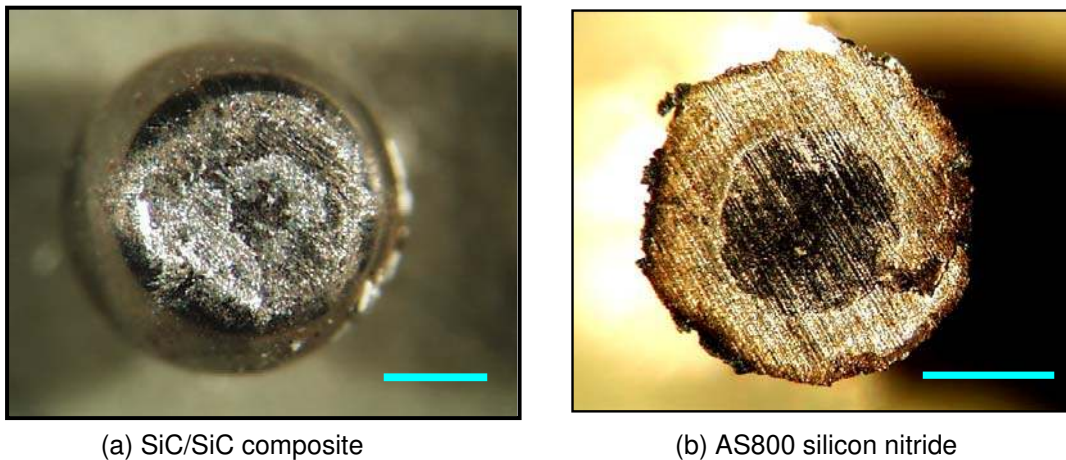(a) SiC/SiC composite   (b) AS800 silicon nitride

Figure 6: Typical examples of 1.59-mm steel ball projectiles showing plastic deformation (flattened) impacted at 350 m/sec at ambient temperature in: (a) SiC/SiC ceramic matrix composite and (b) AS800 silicon nitride (reference 15). Bar = 500 µm.

The front impact damage generated in target specimens was in a form of craters associated with breakage of matrices and fiber tows at impact sites. Figure 7 presents the front impact damage size as function of impact velocity. Front damage size was somewhat insensitive to the type of specimen support particularly at 1316°C. However, in terms of temperature, front damage size was greater at 1316°C than at 25°C, regardless of the type of specimen support, attributed to a 'softening' effect of the composite at the elevated temperature. At higher impact velocities $\geq$350 m/sec, backside damage became significant for the partially supported specimens with a presence of severe backside cracking and delamination, due to the backside tensile

stresses induced by flexure. By contrast, no visible backside damage was observed for the fully supported specimens. Typical examples of backside damages aforementioned, generated at low (around 200 m/sec) and high (around 400 m/sec) impact velocities in full and partial supports, are presented in figures 8 and 9, respectively, for 25°C and 1316°C. Figure 10 is for front impact damages at 25°C and 1316°C for full support. Note that the figures for 1316°C in figure 10 were taken after post-impact strength testing and that the front damages were still intact despite a presence of cracking induced by post-impact strength testing.
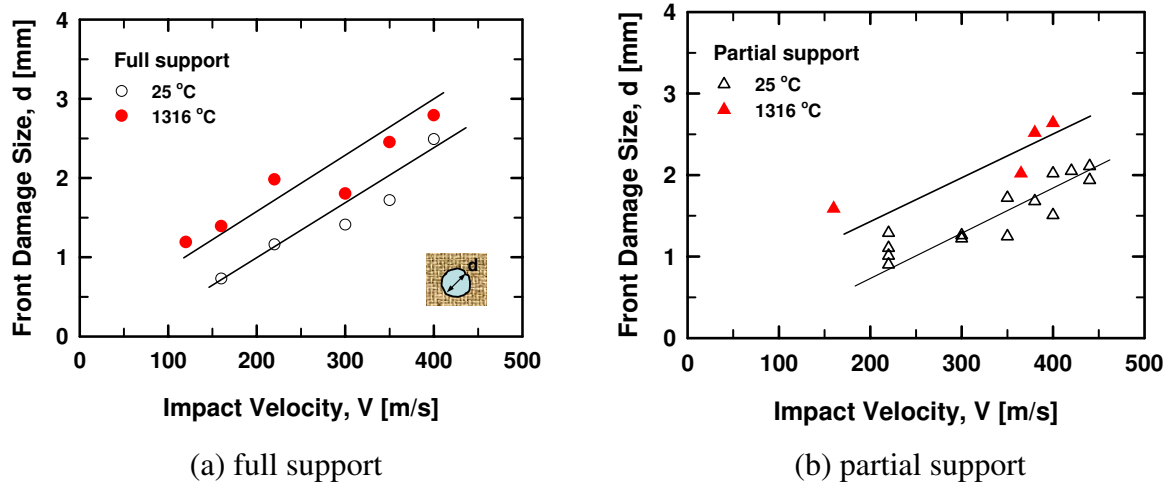

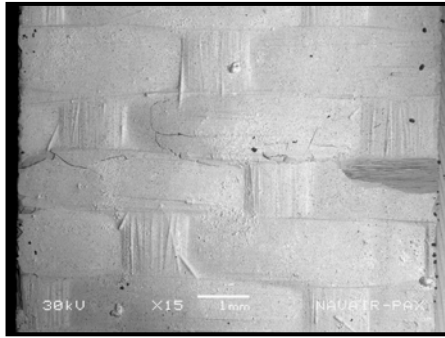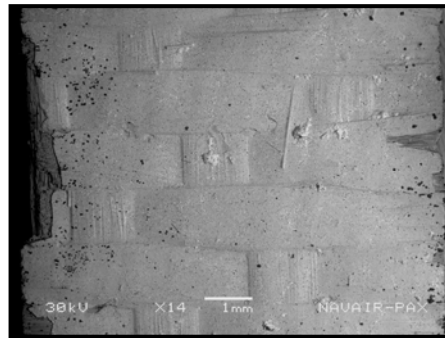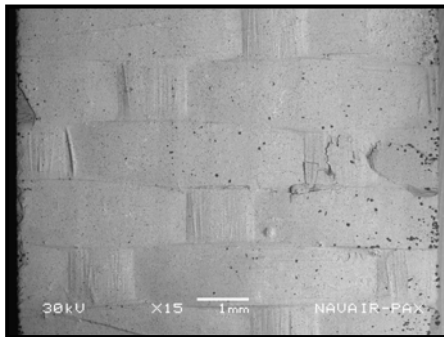(a) full support   (b) partial support

Figure 7: Front impact damage size as a function of impact velocity for SiC/SiC ceramic matrix composite impacted by 1.59-mm steel ball projectiles in: (a) full support and (b) partial support.
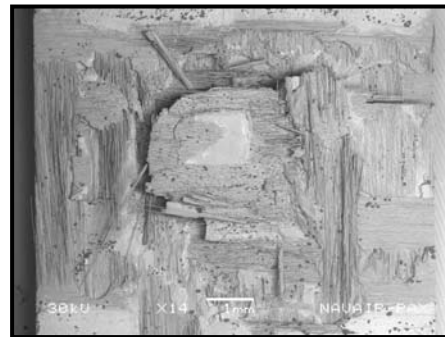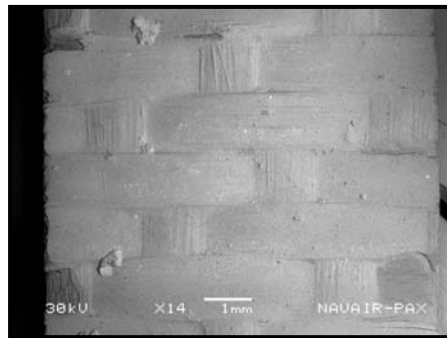
V = 160 m/sec

V = 160 m/sec

V = 400 m/sec

V = 440 m/sec

(a) full support

(b) partial support

Figure 8: Typical examples of backside impact damages in SiC/SiC CMC impacted at low (160 m/sec) and high (400-440 m/sec) velocities by 1.59-mm steel ball projectiles at ambient temperature in: (a) full support and (b) partial support. Note difference in damage between two supports at high impact velocities.

V = 160 m/sec

V = 220 m/sec

V = 400 m/sec

V = 380 m/sec

(a) full support
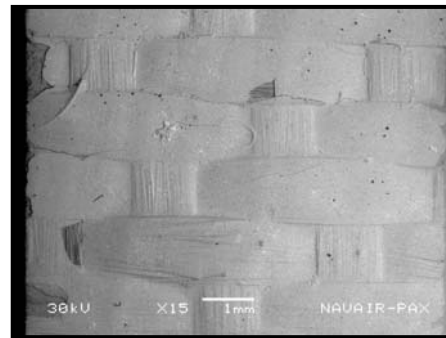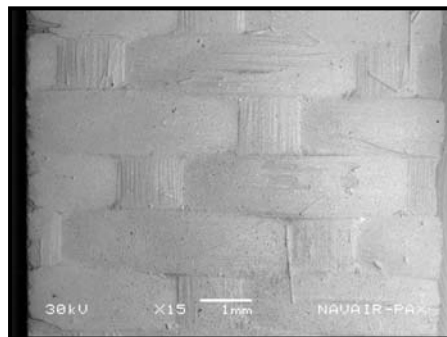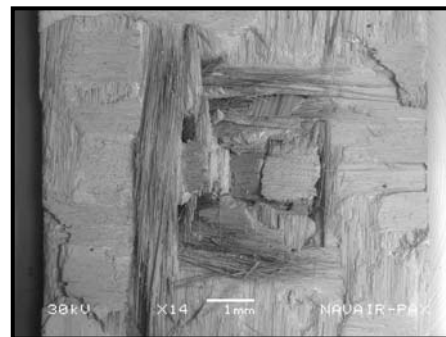
(b) partial support

Figure 9: Typical examples of backside impact damages in SiC/SiC CMC impacted at low (160-220 m/sec) and high (380-400 m/sec) velocities by 1.59-mm steel ball projectiles at 1316°C in: (a) full support and (b) partial support. Note difference in damage between two supports at high impact velocities.
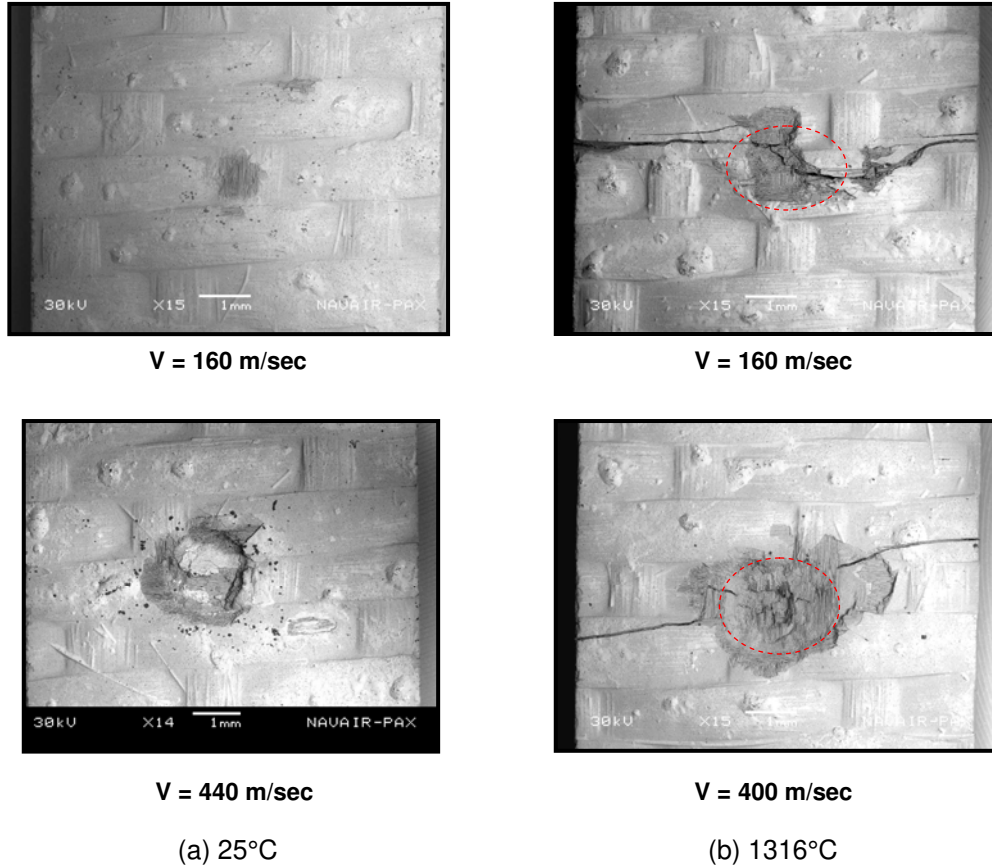
Figure 10: Typical examples of front impact damages in SiC/SiC CMC impacted at low (160 m/sec) and high (400-440 m/sec) velocities by 1.59-mm steel ball projectiles in full support at: (a) ambient temperature (25°C) and (b) 1316°C. Note that elevated-temperature target specimens were strength-tested thus showing the resulting failure cracks. The dotted circles indicate impact damages prior to post-impact strength testing.

A cross-sectional view containing the impact site of a target specimen impacted at 400 m/sec in partial support at 25°C is shown in figure 11. Also included in the figure are the front and back sides of the target specimen prior to sectioning. A minor front but severe backside damages with some delamination are evident, showing even some material removal from the backside. Also important is the formation of cone cracks initiating from the impact site, making damage more significant at the backside than at the front impact site and letting the material beneath the impact site be displaced toward the backside. The angle of the cone cracks was about 120 deg. Generation of cone cracks by spherical projectiles has been observed in monolithic silicon nitrides (references 4, 9, 15, 16, 17, and 19) and is typified of many brittle solids including glass dynamically (references 1, 2, and 5) or statically (reference 8). One example such as in AS800 silicon nitride is shown in figure 12 (reference 16), where the contour of a well-developed cone crack is seen from the fracture surface, together with a *volcanic-island* like cone

completely separated from the specimen. The specimen was in 2-mm thick disk and subjected to 1.59-mm steel ball impact at 400 m/sec at 25°C in full support. The cone angle was about 80 deg. The SiC/SiC composite shown in figure 11, in fact, was on the verge of being penetrated by the projectile. A complete penetration of a SiC/SiC target specimen was observed at an impact velocity 440 m/sec with a well-developed through-the-thickness cone crack that was clearly revealed via computed tomography (CT), as shown in figure 13 (reference 20). Hence, a formation of cone cracks is one of the key damage phenomenon associated with spherical projectiles, regardless of type of materials. Progressive impact damage with increasing impact velocity thus aforementioned was summarized in figure 14 for both types of specimen support.

Impact site   Backside

(a)

Impact site

(b)
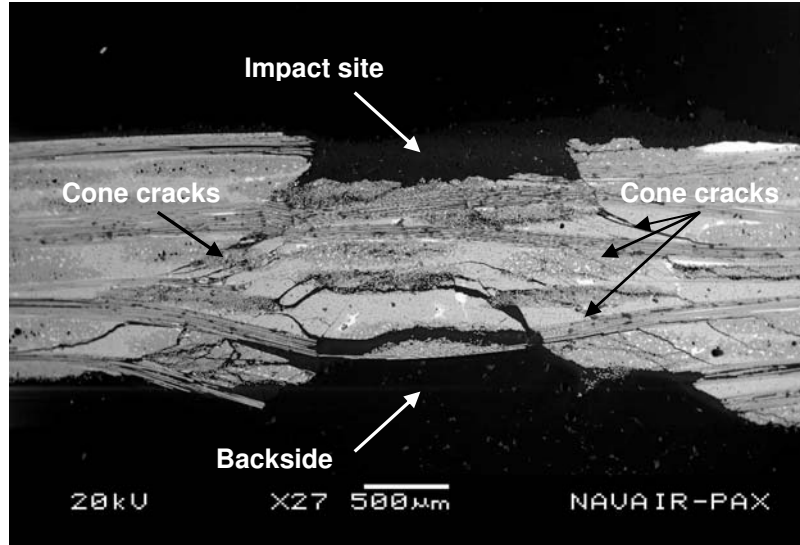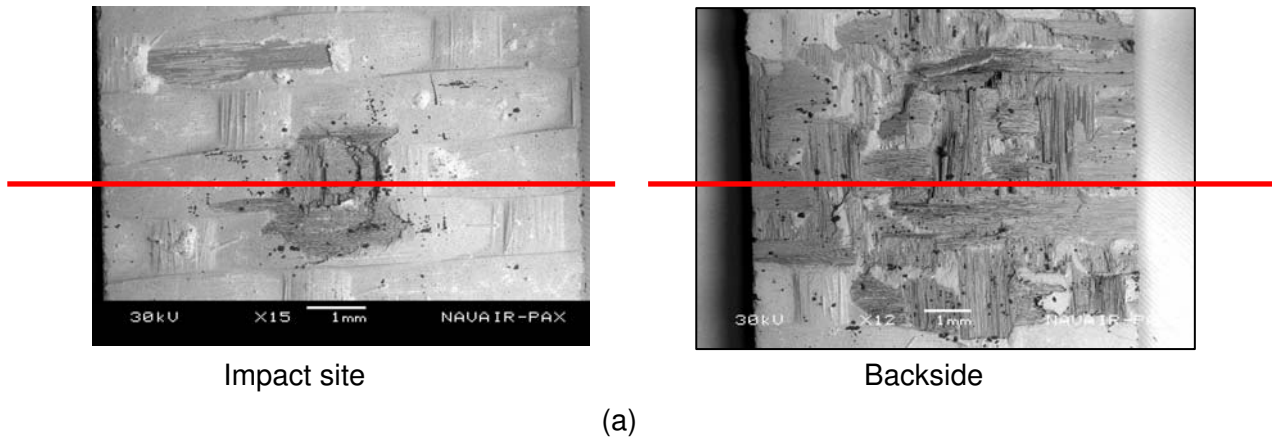
Figure 11: (a) Front impact and backside damages and (b) cross-sectional view of the impact site of a SiC/SiC target specimen impacted at 400 m/sec by 1.59-mm steel ball projectile at ambient temperature. Lines in (a) indicate the related sectioning. Angle of cone cracks ≈ 120 deg.

Impact site
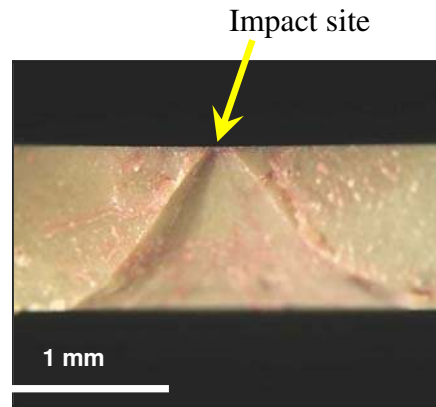
(a) Fracture surface

(b) A separated cone from (a)

Figure 12: (a) Fracture surface and (b) a separated cone of an AS800 silicon nitride target specimen (disk) impacted at 400 m/sec by 1.59-mm steel ball projectile at ambient temperature. Angle of cone $\approx$ 80 deg.

Figure 13: CT images of a SiC/SiC target specimen impacted at 440 m/sec by 1.59-mm steel ball projectile at ambient temperature. Well-developed cone cracking is noted.

Figure 14: Schematics of damage progress from low (top) to high (bottom) impact velocities in: (a) full support and (b) partial support. The vertical arrows indicate a case of increase in impact velocity.

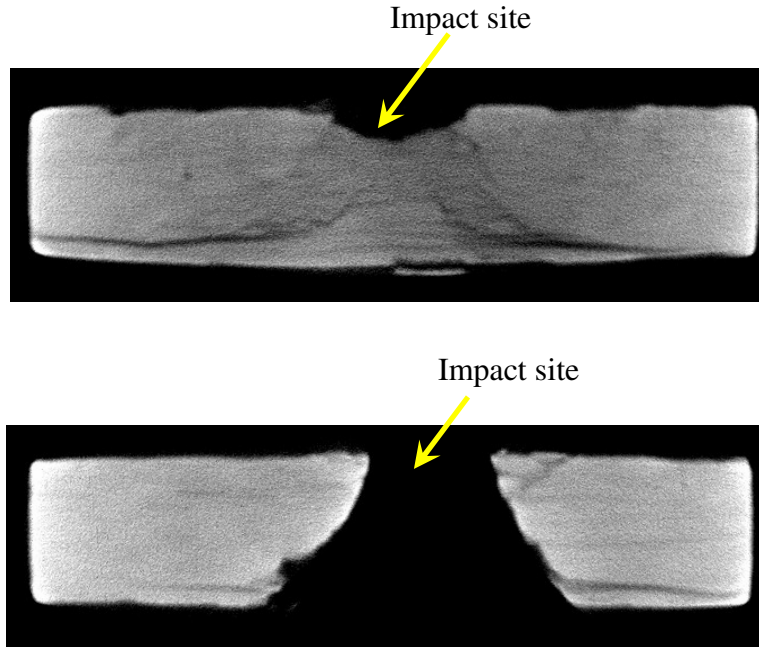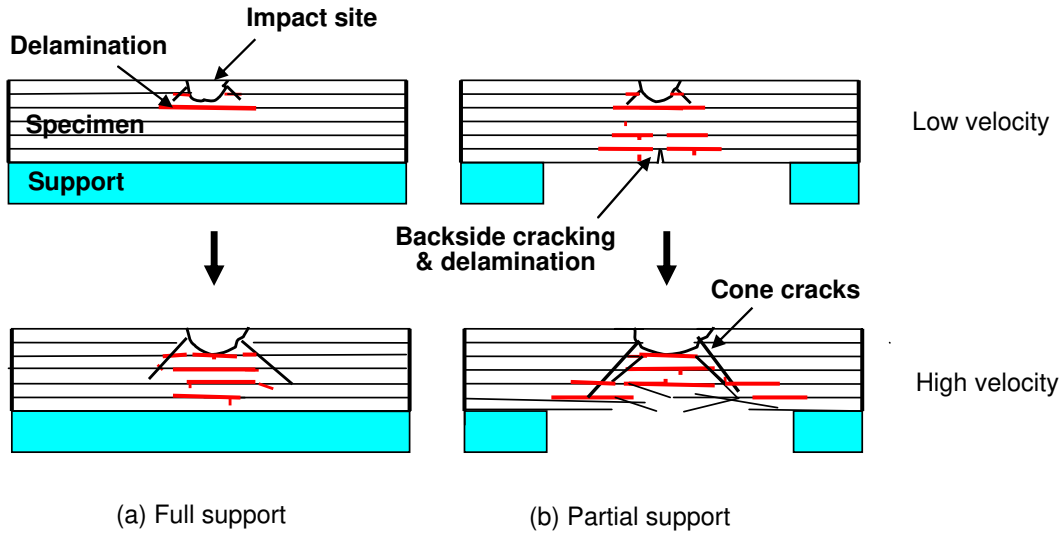Despite the nonexistence of backside tensile stress, fully supported specimens still exhibited significant delamination damage particularly at higher impact velocities ≥ 350 m/sec, which further reduced their residual strength. Such degree of delamination was different from that observed under static loading condition. The delamination damage is believed to be due in part to interactions of traveling stress waves (reference 21). The occurrence of this impact induced delamination suggests that resistance to impact might be enhanced by improving interlaminar properties of the composites. The related properties include interlaminar tensile and shear strengths, and/or interlaminar modes I and II fracture resistances (G_I and G_{II}) (reference 22).

In terms of fractography, the SiC/SiC composite rendered a daunting challenge to detail the impact damages, attributed to its complex 2-D woven architecture as well as to dissimilar constituents of materials. Contrast to the case for monolithic ceramics, conventional optical, and/or SEM examinations for the SiC/SiC composite may not be sufficient in many cases. Additional use of pertinent nondestructive evaluation tools such as CT and/or pulsed thermography techniques (reference 23) is strongly recommended for fiber-reinforced CMCs. The morphological approaches described above can give qualitative information pertaining to impact damage. However, they do not provide quantitative assessments as to how impact damage result in strength degradation as a function of impact variables such as velocity, type of support, and temperature. This will be described in the following section.

3.2 POST-IMPACT STRENGTH (RESIDUAL STRENGTH)

Results of strength testing for impacted target specimens are presented in figure 15, where post-impact flexure strength was presented as a function of impact velocity for both types of specimen support at each temperature. Included in figure 15 is the as-received (AsR) flexure strength (=578 ±56 MPa) determined at ambient temperature. Target specimens impacted failed from their impact sites (see, for example, figure 10). Exception to this was that one specimen at each temperature impacted at the lowest velocity (i.e., 160 m/sec at 25°C and 115 m/sec at 1316°C) did not fracture from impact site because of its negligible impact damage. The resulting strength of these specimens was close to the AsR strength. As seen in the figure, post-impact strength decreased with increasing impact velocity at both temperatures, regardless of the type of specimen support, due to impact damage increasing with impact velocity. It is also peculiar that the post-impact strength was almost a linear function of impact velocity. As expected, for a given impact velocity, strength degradation was greater for the partially supported specimens than for the fully supported counterparts, as mentioned in the Impact Damage Morphology section. Difference in strength degradation between 25°C and 1316°C was significant for the partially supported particularly at higher impact velocities ≥ 350 m/sec, while the difference appeared to be insignificant for the fully supported specimens.
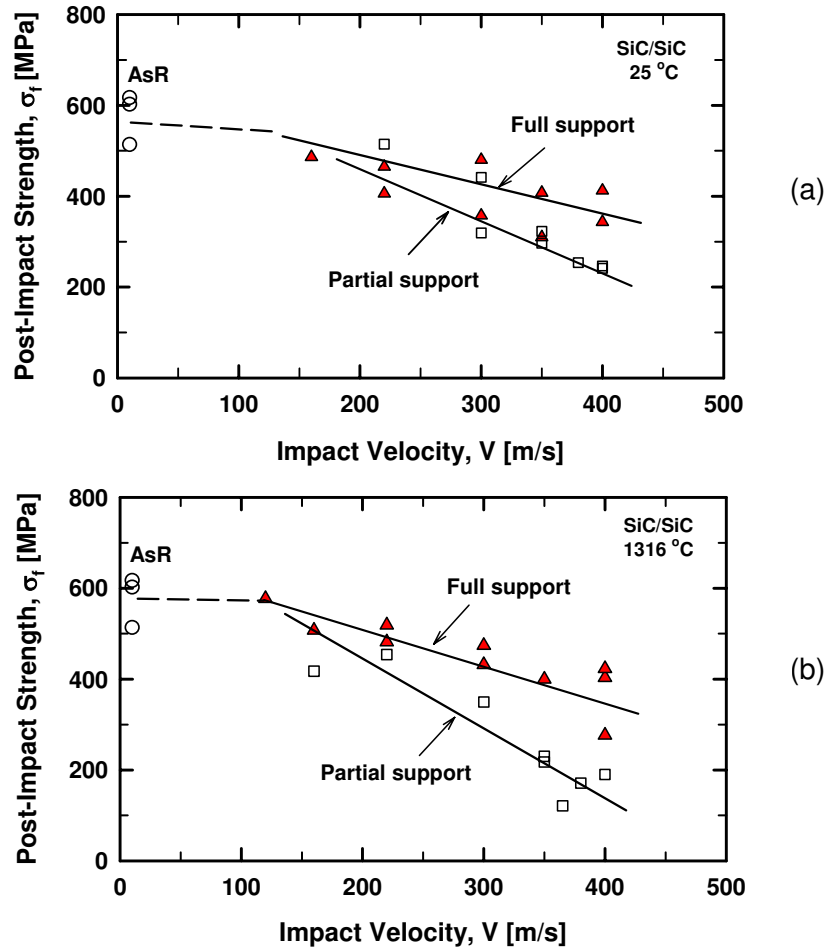
Figure 15: Post-impact strength as a function of impact velocity for SiC/SiC CMC impacted by 1.59-mm diameter steel ball projectiles with two different types of specimen support at: (a) Ambient temperature (25°C) and (b) 1316°C. AsR = As-received strength determined at ambient temperature with no impact.

Figure 16 shows typical load-displacement curves determined in post-impact testing for partially supported specimens impacted at 25°C. Progressive decrease in both stiffness and strength is manifest with increasing impact velocity from 220 to 400 m/sec, again indicative of increasing severity of impact damage. A similar trend has also been observed for fully supported specimens (reference 18). However, the degree of change in stiffness was somewhat less noticeable for fully supported specimens, compared to partially supported counterparts, because of less impact damage associated with the fully supported.
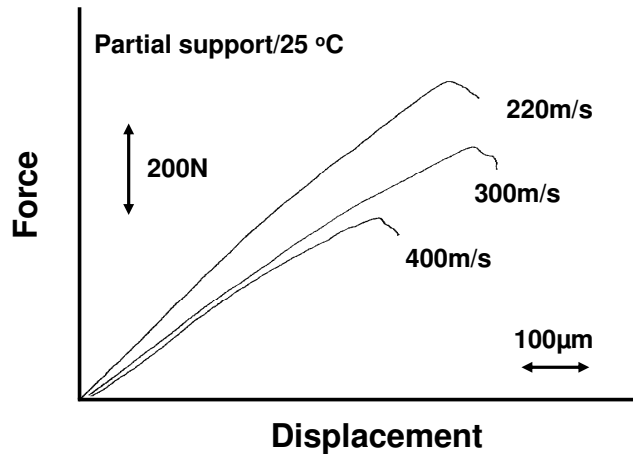

Figure 16: Typical force-versus-displacement curves in flexure determined from SiC/SiC target specimens impacted at three different velocities by 1.59-mm steel ball projectiles in partial support at ambient temperature (25°C). The peak of each curve indicates a fracture force.

3.3 COMPARISON IN FOREIGN OBJECT DAMAGE BETWEEN SiC/SiC COMPOSITE AND SILICON NITRIDES

Figure 17 shows a comparison in normalized post-impact strength ($\bar{\sigma}_f$) as a function of impact velocity between the current SiC/SiC composite and the two gas-turbine grade silicon nitrides, AS800 and SN282 (reference 25). Post-impact strength of each material was normalized with respect to its respective as-received strength (=640±42, 513±64 MPa for AS800 and SN282, respectively). Flexure target specimens of AS800 and SN282, 4-mm wide, 25-mm long, and 2.0-mm thick, were impacted by 1.59-mm steel ball projectiles in full support and their post-impact strength was determined as a function of impact velocity (reference 24). For a given material, a total of 10 target specimens was used at each velocity. The critical impact velocity (V_c), defined as a velocity where all target specimens were subjected to catastrophic fracture upon impact, was well established for the two silicon nitrides as follows:

$$V_c = 260 \text{ m/sec for AS800}$$
$$V_c = 180 \text{ m/sec for SN282}$$

By contrast, as seen in figure 17, such a V_c was not defined in the SiC/SiC composite even up to an impact velocity of 400 m/sec. Furthermore, the SiC/SiC composite exhibited greater tolerance to impact damage with monotonic strength degradation at velocities $\geq$220 m/sec than either AS800 or SN282 silicon nitride. A similar result was also observed by van Roode et al. (reference 11). However, it must be noted that the impact damages generated in the SiC/SiC composite at high impact velocities >350 m/sec are still undesirable in view of performance and structural integrity of aeroengines when CMC airfoils are considered as turbine components.

Figure 17: Comparison of normalized post-impact strength as a function of impact velocity between SiC/SiC composite and AS800 and SN282 silicon nitrides (2 mm thick) (reference 24) impacted in full support at ambient temperature (25°C). V_c is where target specimens fracture catastrophically upon impact.

Figure 18 shows normalized post-impact strength ($\bar{\sigma}_f$) as a function of kinetic impact energy (U_k) for the data on the SiC/SiC composite and AS800 and SN282 silicon nitrides in figure 17. Kinetic impact energy, U_k, was defined as

$$U_k = \frac{1}{2}mV^2 \tag{1}$$

where m is the mass of steel ball projectile. Similar to the trend shown in figure 17, monotonic degradation in strength with increasing impact energy was typified for the SiC/SiC composite, while significant strength degradation was exemplified for AS800 and SN282 silicon nitrides at U_k>0.2J and U_k>0.3J, respectively. The critical kinetic impact energy (U_{kc}), where all target specimens failed upon impact, was U_{kc}=0.56J and 0.27J for AS800 and SN282 silicon nitrides,

respectively. The SiC/SiC composite, without U_{kc}, yielded a best-fit relationship between $\bar{\sigma}_f$ and U_k:

$$\bar{\sigma}_f = 0.66\, U_k^{-0.15} \tag{2}$$

The Hertzian contact stress analysis in conjunction with fracture mechanics for dense, homogeneous, isotropic brittle elastic solids gives the following relation (reference 1):

$$\bar{\sigma}_f = \Phi'' U_K^{-0.20} \tag{3}$$

The SiC/SiC composite showed somewhat reasonable agreement (0.15 versus 0.20) in slope with the Hertzian contact stress theory. However, this does not mean the material respond to projectile impact like a homogeneous, isotropic elastic body. The previous studies (references 15, 16, and 17), in fact, indicated that the data on both AS800 and SN282 exhibited a significant deviation from the contact stress theory, as also seen from the data in figure 18. A model to predict FOD and strength degradation in CMCs is thus a prerequisite.
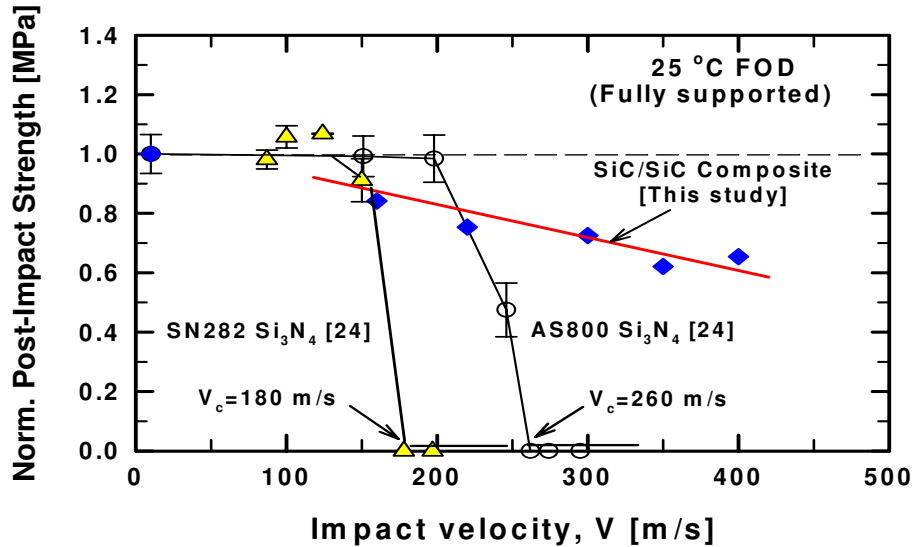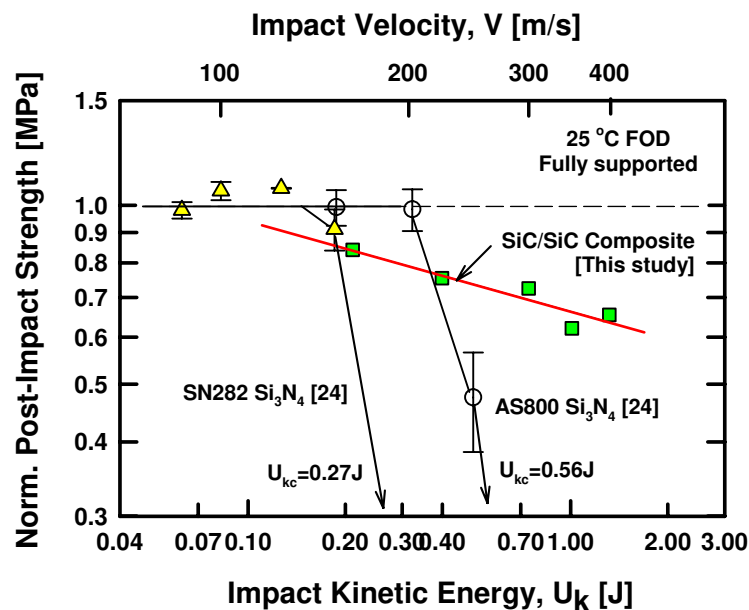

Figure 18: Comparison of normalized post-impact strength as a function of impact kinetic energy between SiC/SiC composite and AS800 and SN282 silicon nitrides (2-mm thick) (reference 24) impacted in full support at ambient temperature (25°C). U_{kc} is a critical impact kinetic energy where target specimens fracture catastrophically upon impact.

3.4 <u>ESTIMATION OF IMPACT FORCE AND BACKSIDE TENSILE STRESS IN PARTIAL SUPPORT</u>[1]

As seen in the foregoing sections, the impact damage was much greater in partial support than in full support, attributed to the existence of tensile stress on the backside of the target specimen. Therefore, it is important to estimate the magnitude of the impact force and tensile stress as a function of impact velocity so that a provision to mitigate backside damage or for design modification could be made. Accurate analytical estimation of impact force and stress is extremely difficult because of the involvements of severe plastic deformation of projectiles, appreciable impact-site damage occurring at higher impact velocities >350 m/sec, and a complex architectural nature of the target material. This violent impact behavior as well as the complexity of a material's structure would be a big hindrance toward theoretical approaches and modeling. In addition, the frictional effects by property (e.g., elastic modulus, Poisson's ratio, etc.) mismatch between dissimilar projectile and target materials and the complexity associated with different material constituents of the target material are also added obstacles. In this section, however, a first order approximation of the impact force and backside tensile stress of a target specimen in partial support is made under some simplifying quasi-static assumptions.

3.4.1 DERIVATION

For a first order approximation, the following simplifying assumptions were made:

a. Impact is under a quasi-static condition. The duration of the impact is relatively long compared with the period of the fundamental natural frequency of the impact bodies.

b. Effect of stress wave interactions in the transverse direction (as well as in the longitudinal direction) is negligible.

c. Material is macroscopically homogeneous.

d. Frictional effect between projectile and target upon impact is of little significance.

e. For a given impact condition, the coefficient of restitution does not vary significantly with impact velocity.

It is also assumed that at any given time the velocity (v) at a point on the target (beam) is proportional to the static deflection (y) such that (see figure 19)

$$\frac{v}{y} = \frac{v_c}{y_c} \tag{4}$$

---

[1] The evaluation of impact force in partial support is of a prime interest and importance in this paper. The impact force in full support has been routinely estimated for many brittle solids in the related communities based on the Hertzian contact theory, so it was not repeated here.

where v_c and y_c are the velocity and deflection, respectively, of the target beam at its center ($x =$ $L/2$). Using $y=P(3L^2x-4x^3)/48EI$ and $y_c=PL^3/48EI$ from the elementary beam theory, where P is the impact force, L is the length of the target, E is the elastic modulus of the target, and I is the
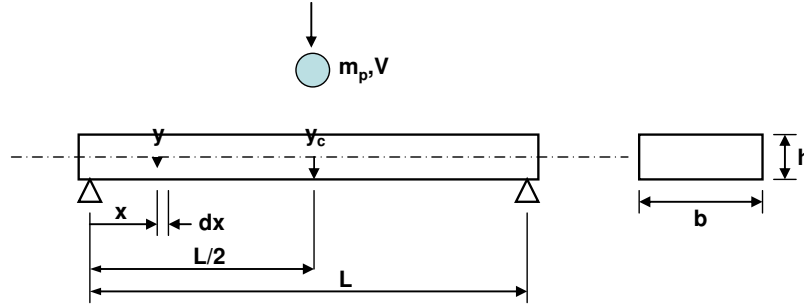

Figure 19: Geometry and configuration of a target beam specimen subjected to projectile impact in partial support

second moment of inertia of the target, the velocity at a point on the target in Equation (4) can be rewritten as

$$v = \frac{(3L^2x - 4x^3)}{L^3} v_c \tag{5}$$

The kinetic energy of the target (U_{kt}) may be determined (reference 25) as

$$U_{kt} = \int_0^L \frac{1}{2}(dm_t)v^2 \tag{6}$$

where $dm_t=\rho A dx$ is an infinitesimal mass of the target with ρ and A being the density and cross-sectional area of the target, respectively. Using dm_t and v in Equation (5), the kinetic energy of the target can be determined as

$$U_{kt} = \frac{1}{2}(\frac{17}{35}m_t)\, v_c^2 \tag{7}$$

where $m_t = \rho AL$. The target is now viewed as a concentrated body of a mass of $(17/35)m_t$. The conservation of linear momentum between the projectile and the target at the first impact event (immediately before and immediately after impact) yields

$$m_pV = (m_p + \frac{17}{35}m_t)\, v_c \tag{8}$$

where m_p is the mass of the projectile, and V is the velocity of the projectile immediately before impact. Solving for v_c in Equation (8) yields

$$v_c = \frac{m_p}{(m_p + \frac{17}{35} m_t)} V \qquad (9)$$

The total kinetic energy (U_{kt}) of the masses of the projectile and target immediately after impact is then

$$U_{kt} = \frac{1}{2}(m_p + \frac{17}{35} m_t) v_c^2$$
$$= \frac{1}{2} \frac{m_p^2}{(m_p + \frac{17}{35} m_t)} V^2 \qquad (10)$$

It is assumed that the projectile and the target are in contact with each other until the target deflects to y_c and then bounce back. The overall energy balance holds as follows:

$$U_k - U_l + U_p = U_{kt} + U_s \qquad (11)$$

where U_k is the kinetic energy of the projectile, U_l is the total energy loss during impact, U_p is the potential energy of the projectile, and U_s are the elastic strain energy of the target, respectively, expressed as follows:

$$U_k = \frac{1}{2} m_p V^2$$
$$U_l = \frac{1}{2} m_p V^2 (1 - e^2)$$
$$U_P = m_p g y_c \qquad (12)$$
$$U_s = \int \frac{1}{2} \sigma \varepsilon \, dV = \frac{1}{2} P y_c$$

The coefficient of restitution in Equation (12), e, is defined as

$$e = - \frac{V_f}{V} \qquad (13)$$

which is the ratio of the final bouncing-back velocity (V_f) immediately after impact to the initial velocity (V) immediately before impact. The coefficient of restitution represents the loss in kinetic energy and is not a basic material property alone. It depends on the geometry of the

bodies, the magnitude of stresses, the type of support, the surface conditions of the bodies, the duration of contact, and material properties. The potential energy of a target after impact is negligible compared to the other energies. Substituting Equations (10) and (12) into Equation (11) using $y_c=PL^3/48EI$, and solving for P give rise to

$$P = 4\sqrt{3}\,V\,[\frac{EI\,m_p}{L^3}]^{1/2}(e^2 - \frac{m_p}{m_p + \frac{17}{35}m_t})^{1/2} \tag{14}$$

The maximum tensile stress (σ_{max}) occurring at $x = L/2$ on the backside of the target is expressed as $\sigma_{max} = Mh/2I$ with $M=PL/4$ (as bending moment) and h being the target thickness. Using these relations together with Equation (14), one can determine the maximum tensile stress as

$$\sigma_{max} = \frac{\sqrt{3}\,V}{2}\,[\frac{Eh^2\,m_p}{IL}]^{1/2}(e^2 - \frac{m_p}{m_p + \frac{17}{35}m_t})^{1/2} \tag{15}$$

Use of $y_c=PL^3/48EI$ and Equation (14) yields the maximum deflection of the target at $x = L/2$ as follows:

$$\delta_{max} = \frac{V}{4\sqrt{3}}\,[\frac{L^3 m_p}{EI}]^{1/2}(e^2 - \frac{m_p}{m_p + \frac{17}{35}m_t})^{1/2} \tag{16}$$

Note that the impact force, maximum tensile stress, and maximum deflection in Equations (14), (15), and (16) are all a linear function of impact velocity, V.

3.4.2 ESTIMATIONS

The following materials' properties, target specimen's dimensions, and its support configuration were used in estimations:

$$m_p = 1.65 \times 10^{-5}\text{ kg; } m_t = 8.45 \times 10^{-4}\text{ kg; } E = 220\text{ GPa}$$
$$L = 20\text{ mm; } h = 2.2\text{ mm; } b = 8\text{ mm}$$

The results of the predicted impact force and maximum tensile stress as a function of the coefficient of restitution (e) are shown in figure 20. For a given impact velocity, both impact force and maximum backside stress are strongly dependent on the coefficient of restitution. The impact force and backside stress seem to be too large when $e \geq 0.5$, compared to the experimental observations. The value of $e=0.3$, which results in $P = 986$ N and $\sigma_{max} = 764$ MPa, appears to reasonable in view of the facts that the backside cracking/damage of the targets was observed significant at $V \geq 350$ m/sec and that the as-received flexure strength of the target was 580

±60 MPa. An example at V=350 m/sec for e=0.3 is presented in the figure. It should be noted that the case for e=0.3 is also indicative of significant decrease in bouncing-back velocity, V_f=105 m/sec. This could be understandable (at least quantitatively) considering the violent impact event at 350 m/sec, accompanying both the appreciable plastic deformation of the projectiles and the higher degree of impact damage generated on the targets, which results in significant loss in the kinetic energy (U_k).
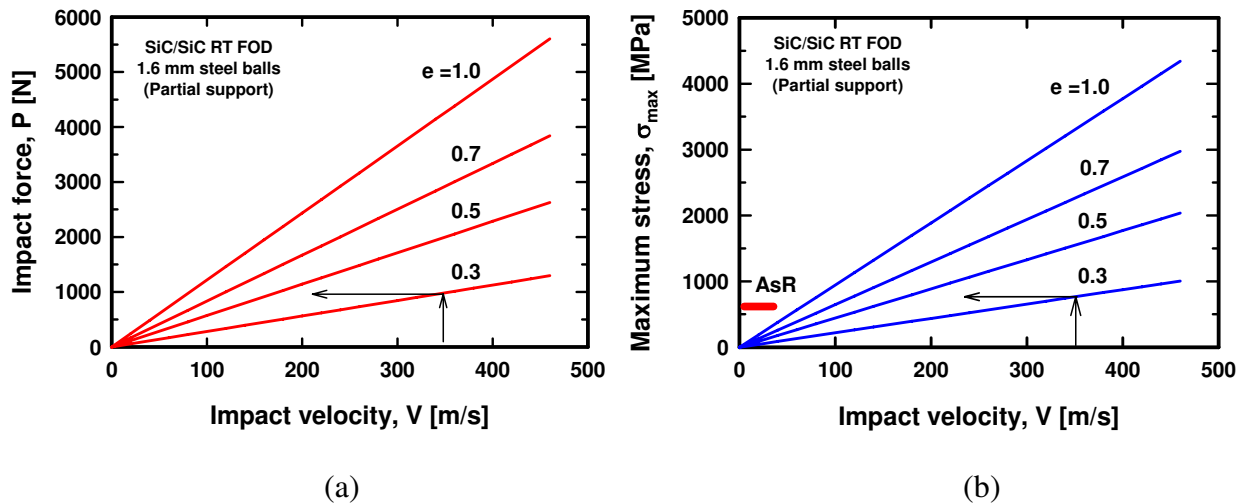

Figure 20: Predicted impact force (a) and maximum backside tensile stress (b) as a function of the coefficient of restitution (e) in SiC/SiC target specimens under a partial support configuration, impact by 1.59-mm diameter steel ball projectiles. An example at V=350 m/sec was indicated with arrows. AsR=As-received strength of target specimens (580 ±60 MPa).

The theoretical approach shown in this work was based on many idealized assumptions and therefore may not provide as a reliable and realistic tool. Pertinent experimental techniques and proper modeling should be sought to determine and assess related dynamic parameters such as force, stresses, deformation, duration of impact, and stress wave interactions. Frictional effects by property (e.g., elastic modulus, Poisson's ratio, etc.) mismatch between dissimilar projectile and target materials, the complexity associated with the target material's architectural nature with different material constituents, and the effect of the coefficient of restitution on impact velocity should be also taken into account. The prospective model(s), albeit daunting in its task, should also be able to predict the mode and degree of damages and their resulting effects on mechanical properties not only in coupon level but also in actual CMC component level.

3.5 <u>IMPLICATIONS</u>

Based on both morphological and post-impact strength results, it can be stated that the type of target specimen support can play a crucial role in determining and controlling the extent of impact damage. This indicates that 3-D CMC airfoils with a thin configuration can be improved in FOD resistance via a proper design by employing a backup type of attachments inside the CMC airfoils, making them into a somewhat full support configuration. Therefore, an appropriate means of design/fabrication should be sought to mitigate impact damage. Some type of '*impact barrier coatings*' is also an alternative to protect CMC substrate as well as to reduce impact-associated contact stresses. A previous study showed that a thin copper foil placed on silicon nitride target specimens gave rise to significant increase in FOD resistance by reducing Hertzian contact stresses (reference 15).

Designing CMC aeroengine components to withstand FOD events is a complex task. Consideration of many factors is required, both in the generation of FOD data as well as in actual component design efforts (reference 19). A sample of major factors to affect FOD includes the following:

$$\Gamma = f(p, t_m, s, i_v, c) \tag{17}$$

where,

Γ = FOD
p = projectile material/geometry/size
t_m = target material/geometry/architecture
s = support and attachment of target
i_v = impact velocity/impact angle/temperature/environment
c = coatings' effect (thermal barrier and/or environmental barrier coatings)

THIS PAGE INTENTIONALLY LEFT BLANK

4. CONCLUSIONS

The overall impact damage of the SiC/SiC composite was found to be greater for partially supported target specimens than for fully supported ones at both 25°C and 1316°C. The strength degradation with respect to impact velocity was more significant at 1316°C, particularly for partially supported target specimens at higher impact velocities.

For fully supported target specimens, frontal contact stresses played a major role in generating damage, while for partially supported ones, both frontal contact and backside flexure stresses were combined sources of damage generation. Cone cracking originating from impact site was also one of the key damage aspects.

Unlike AS800 and SN282 silicon nitrides, the SiC/SiC composite did not yield a V_c where target specimens fractures catastrophically upon impact. This indicates that enhanced FOD resistance could be achieved with the SiC/SiC composite even up to an impact velocity of 400 m/sec. However, the damage generated in the composite, particularly at ≥ 350 m/sec in a partial support configuration, was still considered appreciable from a structural and component performance point of view.

The quasi-static prediction of impact force and corresponding backside tensile stress in partial support was in reasonable agreement with experimental observations, although rigorous experimental verifications are yet to be done.

THIS PAGE INTENTIONALLY LEFT BLANK

REFERENCES

1. Wiederhorn, S. M., and Lawn, B.R., 1977, "Strength Degradation of Glass Resulting from Impact with Spheres," J. Am. Ceram. Soc., 60, pp. 451-458.

2. Wiederhorn, S. M., and Lawn B. R., 1979, "Strength Degradation of Glass Impact with Sharp Particles: I, Annealed Surfaces," J. Am. Ceram. Soc., 62, pp. 66-70.

3. Ritter, J. E., Choi,S. R., Jakus, K, Whalen, P. J., and Rateick, R. G., 1991, "Effect of Microstructure on the Erosion and Impact Damage of Sintered Silicon Nitride," J. Mater. Sci., 26, pp. 5543-5546.

4. Akimune, Y, Katano, Y, and Matoba, K, 1989, "Spherical-Impact Damage and Strength Degradation in Silicon Nitrides for Automobile Turbocharger Rotors," J. Am. Ceram. Soc., 72, pp. 1422-1428.

5. Knight, C. G., Swain, M. V., and Chaudhri, M. M., 1977, "Impact of Small Steel Spheres on Glass Surfaces," J. Mater. Sci., 12, pp.1573-1586.

6. Rajendran, A. M., and Kroupa, J. L., 1989, "Impact Design Model for Ceramic Materials," J. Appl. Phys, 66, pp. 3560-3565.

7. Taylor, L. N., Chen, E. P., and Kuszmaul, J. S., 1986 "Microcrack-Induced Damage Accumulation in Brittle Rock under Dynamic Loading," Comp. Meth. Appl. Mech. Eng., 55, pp. 301-320.

8. Mouginot, R., and Maugis, D., 1985, "Fracture Indentation beneath Flat and Spherical Punches," J. Mater. Sci., 20, pp. 4354-4376.

9. Evans, A. G., and Wilshaw, T. R., 1977, "Dynamic Solid Particle Damage in Brittle Materials: An Appraisal," J. Mater. Sci., 12, pp. 97-116.

10. Liaw, B. M., Kobayashi, A. S., and Emery, A. G., 1984, "Theoretical Model of Impact Damage in Structural Ceramics," J. Am. Ceram. Soc., 67, pp. 544-548.

11. van Roode, M., et al., 2002, "Ceramic Gas Turbine Materials Impact Evaluation," ASME Paper No. GT2002-30505.

12. Richerson, D. W., and Johansen, K. M., 1982, "Ceramic Gas Turbine Engine Demonstration Program," Final Report, DARPA/Navy Contract N00024-76-C-5352, Garrett Report 21-4410.

13. Boyd, G. L., and Kreiner, D. M., 1987, "AGT101/ATTAP Ceramic Technology Development," Proceeding of the Twenty-Fifth Automotive Technology Development Contractors' Coordination Meeting, p.101.

14. van Roode, M., Brentnall, W. D., Smith, K. O., Edwards, B., McClain, J., and Price, J. R., 1997, "Ceramic Stationary Gas Turbine Development – Fourth Annual Summary," ASME Paper No. 97-GT-317.

15. (a) Choi, S. R., Pereira, J. M., Janosik, L. A., and Bhatt, R. T., 2002, "Foreign Object Damage of Two Gas-Turbine Grade Silicon Nitrides at Ambient Temperature," Ceram. Eng. Sci. Proc., 23, pp. 193-202; (b) Choi, S. R., et al., 2004, "Foreign Object Damage in Flexure Bars of Two Gas-Turbine Grade Silicon Nitrides," Mater. Sci. Eng. A 379, pp. 411-419.

16. (a) Choi, S. R., Pereira, J. M., Janosik, L. A., and Bhatt, R. T., 2003, "Foreign Object Damage of Two Gas-Turbine Grade Silicon Nitrides in a Thin Disk Configuration," ASME Paper No. GT2003-38544; (b) Choi, S. R., et al., 2004, "Foreign Object Damage in Disks of Gas-Turbine-Grade Silicon Nitrides by Steel Ball Projectiles at Ambient Temperature," J. Mater. Sci., 39, pp. 6173-6182.

17. (a) Choi, S. R., et al., 2005, "Effect of Projectile Materials on Foreign Object Damage of a Gas-Turbine Grade Silicon Nitride," ASME Paper No. GT2005-68866; (b) Choi, S. R., et al., 2006, "Foreign Object Damage in a Gas-Turbine Grade Silicon Nitride by Spherical Projectiles of Various Materials," NASA TM-2006-214330, NASA Glenn Research Center, Cleveland, OH.

18. Choi, S. R, Bhatt, R. T., Perrira, J. M., and Gyekenyesi, J. P., 2004, "Foreign Object Damage Behavior of a SiC/SiC Composite at Ambient and Elevated Temperatures," ASME Paper No. GT2004-53910.

19. Peralta and Yoshida, H., 2003, Ceramic Gas Turbine Component Development and Characterization, van Roode, M, Ferber, M. K., and Richerson, D. W., eds., Vol. 2, pp. 665-692, ASME, New York, NY.

20. Cosgriff, L. M., 2004, Unpublished work, NASA Glenn Research Center, Cleveland, OH.

21. Sierakowski, R. L., 2000, "Impact Damage-Tolerant Composite Structural Design," pp. 106-132 in Impact Behavior of Fiber-Reinforced Composite Materials and Structures, Edited by Reid, S. R. and Zhou, G., Woodhead Publishing Limited, Cambridge, England.

22. Choi, S. R. and Kowalik, R. W., 2007, "Interlaminar Crack Growth Resistances of Various Ceramic Matrix Composites in Mode I and Mode II Loading," ASME Paper No. GT2007-27080; also in J. Eng. Gas Turbines & Power, Vol. 130, 031301, 2008.

23. Cosgriff, L. M., Bhatt, R., Choi, S. R., Fox, D. S., 2005, "Thermographic Characterization of Impact Damage in SiC/SiC Composite Materials," Proc. SPIE, Vol. 5767, pp. 363-372 in Nondestructive Evaluation and Health Monitoring of Aerospace Materials, Composites, and Civil Structure IV.

24. Racz, Z., and Choi, S. R., 2005, Unpublished work, NASA Glenn Research Center, Cleveland, OH, 2004.

25. D'Isa, F. A., 1968, <u>Mechanics of Metals</u>, Chapter 7, Addison-Wesley Publishing Co., Reading, MA.

THIS PAGE INTENTIONALLY LEFT BLANK

DISTRIBUTION:

Office of Naval Research, Dr. David A. Shifler, 875 N. Randolph Street   (1)
    Suite 1425/ONR 332, Arlington, VA 22203
NAVAIRWARCENACDIV (4.3.4.1/Choi), Bldg. 2188, Room 101A   (25)
    48066 Shaw Road, Patuxent River, MD 20670
NAVAIRSYSCOM (AIR-5.1), Bldg. 304, Room 100   (1)
    22541 Millstone Road, Patuxent River, MD 20670-1606
NAVAIRWARCENACDIV (4.12.4.3), Bldg. 407, Room 116   (1)
    22269 Cedar Point Road, Patuxent River, MD 20670-1120
NAVTESTWINGLANT (55TW01A), Bldg. 304, Room 200   (1)
    22541 Millstone Road, Patuxent River, MD 20670-1606
DTIC   (1)
    Suite 0944, 8725 John J. Kingman Road, Ft. Belvoir, VA 22060-6218